Sustainable Structures
ISSN: 2789-3111 (Print); ISSN: 2789-312X (Online)
http://www.sustain-dpl.com/journal/sust
DOI: 10.54113/j.sust.2026.000117

***ORIGINAL ARTICLE***

# Eco-friendly geopolymer composites: leveraging parawood ash for sustainable construction materials

**Abideng Hawa[a,*], Preecha Salaemae[a], Woraphot Prachasaree[b]**

[a]Infrastructure and Materials Innovation Research Unit, Department of Civil Engineering, Princess of Naradhiwas University, Narathiwat 96000, Thailand
[b]Department of Civil Engineering, Prince of Songkla University, Songkhla 90110, Thailand
[*]Corresponding Author: Abideng Hawa. Email: dr.abideng@pnu.ac.th

**Abstract:** Biomass is gaining in popularity as an energy source. However, the combustion process generates a significant amount of ash, posing an environmental challenge. Previous studies have explored the incorporation of biomass ash into cement concrete to reduce its environmental impact; however, this has resulted in reduced strength performance. Biomass ash has been increasingly used as a component of geopolymer binder materials. This research examined how the treatment processes influence the physical and mechanical properties of geopolymer mortars that include parawood ash and fly ash. The parawood ash was mixed at 0%, 20%, 40%, and 60% by weight of the binder, and the specimens were subjected to heat curing at 80°C for 6, 12, and 24 h and cured at ambient temperature (30 ± 2°C) for 24 h. The compressive strength, bulk density, compressive strength loss after immersion in seawater, microstructure, chemical composition, and mineral composition of the test specimens were evaluated. The results demonstrated significant improvements in compressive strength. The geopolymer specimens with 20% parawood ash, cured at ambient temperature for 24 h, achieved the highest compressive strength of 32.31 MPa at 28 days. However, the specimens subjected to heat curing for 6-24 hours exhibited optimal compressive strengths within the first 24 h. Prolonged heat curing also effectively reduced the bulk density of the geopolymer. In addition to enhancing the compressive strength, the incorporation of parawood ash contributes to the reduction of waste materials.

**Keywords:** biomass, geopolymer, fly ash, parawood ash, microstructure

## 1 Introduction

The generation of electricity from biomass as a substitute for fossil fuels is of significant importance in the context of global warming, because it can reduce carbon emissions. Amidst the global calls for countries to reduce their carbon emissions, biomass power generation has regained prominence. Over the past two decades, from 2000 to 2020, electricity production from biomass power plants has increased from 162 to 685 TWh [1]. Asia and Europe lead biomass electricity production, generating 276 TWh and 238 TWh, respectively, with Europe accounting for 14% of renewable electricity production [1]. However, this rapid growth has led to a significant increase in biomass ash production.

In Thailand, various agricultural waste materials are utilized as biomass fuels for electricity generation, such as rice husks and bagasse, among others. Currently, there has been an expansion in electricity production using parawood, as Thailand possesses extensive para rubber tree plantations and



Received: 24 December 2025; Received in revised form: 4 July 2026; Accepted: 8 July 2026

is one of the world's leading producers of para rubber. In the para rubber tree cultivation cycle, when the trees reach an advanced age, they must be cut down and replaced with new plantings. The residual parawood from furniture production is used as biomass fuel in biomass power plants, leading to an annual increase in parawood ash (PWA) production. In 2024, Thailand generated approximately 6.4 million tonnes of para rubber wood for use as biomass fuel [2]. The combustion of para rubber wood yields a residual ash content of approximately 2% by weight, resulting in an estimated 0.128 million tonnes of rubber wood ash (RWA). Currently, these ash by-products are only partially disposed of or utilized.

One of the most commonly used and effective binding agents for geopolymer applications is fly ash, a residual product from coal-fired power plants that generate electricity [3-6]. Many researchers have investigated the integration of fly ash with various industrial waste materials, including slag [7-9], metakaolin [10-12], palm oil ash [13, 14], rice husk ash [15-17], and bagasse ash [18, 19]. In addition to the utilization of the aforementioned waste materials, recent studies have explored the incorporation of biomass power plant wood ash as a component in geopolymer production, either as a replacement for fly ash [20] or metakaolin [21]. Abdulkareem et al. [22] investigated the potential of utilizing high calcium biomass wood ash as a sustainable substitute for FA Ash in the development of a geopolymer mortar system. Given the environmental and economic benefits of using waste materials like biomass wood ash, the study aimed to evaluate its feasibility as a replacement for FA. The engineering characteristics of mortar samples were evaluated by substituting FA with biomass wood ash in proportions of 10%, 20%, and 30% of the total binder weight. The findings revealed that the geopolymer mixture with 10% biomass wood ash exhibited superior properties compared to the control mix, making it the most effective formulation. At a 20% replacement ratio, the mixture still achieved a compressive strength exceeding 30 MPa, indicating acceptable performance despite the increased biomass wood ash content. However, the geopolymer blend containing 30% biomass wood ash demonstrated notably inferior mechanical properties across all testing periods, highlighting the limitations of higher replacement ratios. Ates et al. [20] reported that a study was conducted on geopolymer fly ash incorporating biomass wood fly ash, both calcined and non-calcined. Testing revealed that the geopolymer mixed with calcined biomass wood fly ash exhibited improved compressive and flexural strength compared to the control geopolymer.

However, it is noteworthy that the use of wood ash as a geopolymer binder has been studied very little compared to other waste materials. For this reason, the researchers are interested in investigating the feasibility of utilizing parawood ash as a component in geopolymer mixtures to mitigate environmental issues.

In this research, geopolymer mortar samples were created by substituting fly ash (FA) with wood pellet ash (WPA) at 20%, 40%, and 60% by weight. These samples underwent various heat treatments, including exposure to 80°C for 6, 12, and 24 hours, as well as ambient temperature curing. The geopolymer binder was activated using a mixture of sodium silicate ($Na_2SiO_3$) and sodium hydroxide (NaOH) solutions, combined by weight. The study examined the compressive strength, water absorption, bulk density and compressive strength loss after immersion in seawater of the blended geopolymer mixes, along with the application of other analytical methods such as scanning electron microscopy (SEM), X-ray fluorescence (XRF), and X-ray diffraction analysis (XRD). The findings and conclusions from this investigation will contribute to a better understanding of waste ash hybridization in producing hybrid waste geopolymers. Additionally, this research may pave the way for the future incorporation of biomass ash in contemporary construction techniques.

## 2 Research and Methodology

### 2.1 Materials

The fly ash was obtained from Mae Moh electric power plant in Lampang province in northern Thailand. The particle size distribution of FA by Malvern laser particle size analyzer is shown in **Fig. 1a**. The chemical compositions and mineral compositions of FA are shown in **Table 1** and **Fig. 2**, respectively. The chemical composition of FA was analyzed using X-ray fluorescence (XRF), revealing that the major oxides were silica ($SiO_2$) and alumina ($Al_2O_3$), while the CaO content was 12.48%. The

X-ray diffraction (XRD) patterns of FA are presented in **Fig. 2**. The mineral phases in fly ash include quartz ($SiO_2$), anhydrite ($Ca(SO_4)$), and magnetite ($Fe_2O_4$). The analysis of the microstructure using scanning electron microscopy (SEM) revealed that the FA exhibits small particle characteristics consistent with the grading test. It is noteworthy that the FA particles are spherical in shape, particularly the silica particles, as shown in **Figs. 3a** and **3b**.

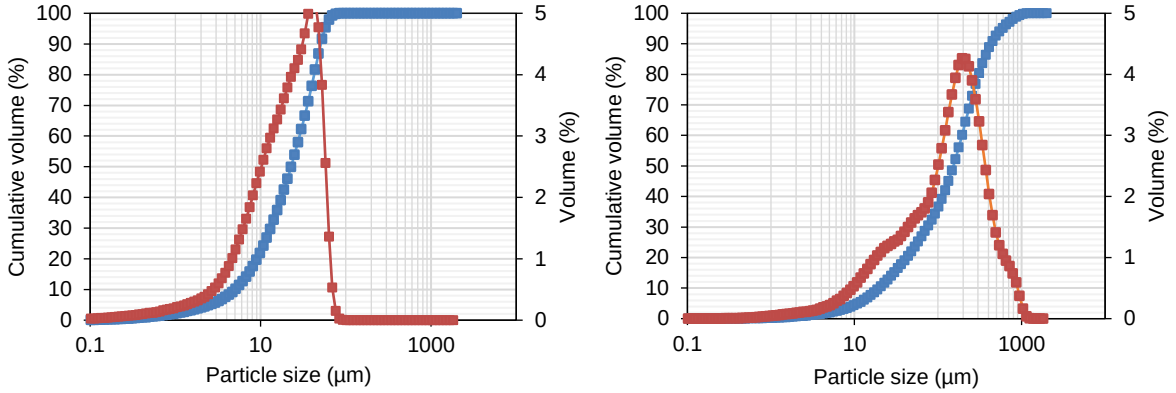


(a) Fly ash (b) Parawood ash

**Fig. 1.** Particle size distribution.

Parawood ash, produced when parawood is burned for electricity generation, was collected from a biomass thermal power facility. This PWA was then processed in a ball mill for about 4 hours. The milling process was conducted at a rotational speed of 33 rpm using a 15 kg steel ball charge. This procedure was maintained to ensure a particle size distribution where at least 66% of the material passed through a 45 μm sieve, thereby satisfying the physical requirements specified in ASTM C618-19. The particle size distributions, as measured by laser scattering, are depicted in **Fig. 1b**. The chemical composition was analyzed using the XRF method, which revealed that PWA contains 34.84% calcium oxide (CaO) and 18.58% potassium oxide ($K_2O$), both of which are the main chemical components. Additionally, other chemical components were also detected, as shown in **Table 1**. **Figs. 3c** and **3d** show the physical characteristics with particles larger than fly ash particles, exhibiting angular shapes and rough surfaces, with flakes adhering to the surface. **Fig. 4** shows the storage of parawood ash after the combustion of parawood and parawood residues from the furniture industry. The image illustrates the large quantities of ash generated, as well as the environmental challenges associated with waste disposal.

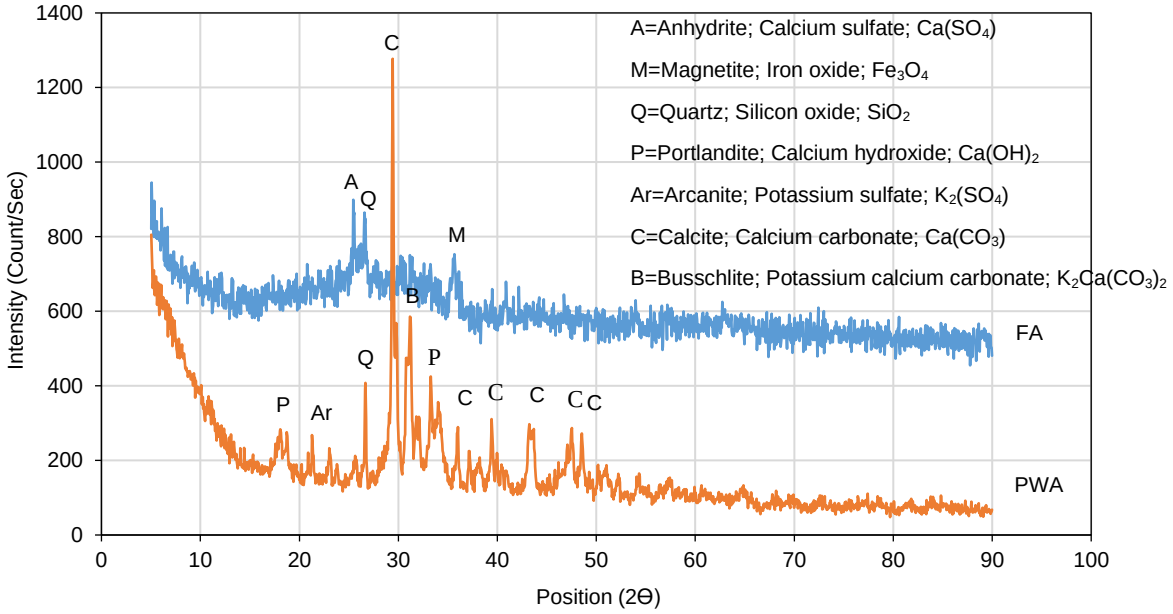


**Fig. 2.** XRD pattern of FA and PWA.

**Table 1.** The chemical composition of FA and PWA.

| Oxides | Content (% weight) | |
|---|---|---|
| | FA | PWA |
| $SiO_2$ | 45.27 | 6 |
| $Al_2O_3$ | 23 | 0.96 |
| $Fe_2O_3$ | 9.4 | 0.52 |
| CaO | 12.48 | 34.86 |
| $K_2O$ | 2.31 | 18.58 |
| $SO_3$ | 2.73 | 4.45 |
| MgO | 1.7 | 4.62 |
| $P_2O_5$ | 0.26 | 2.22 |
| MnO | 0.1 | 0.65 |
| SrO | 0.1 | 0.16 |
| $TiO_2$ | 0.39 | - |
| $Na_2O$ | 1.03 | - |
| $ZrO_2$ | 0.03 | - |
| Cl | - | 0.29 |
| $Rb_2O$ | - | 0.14 |

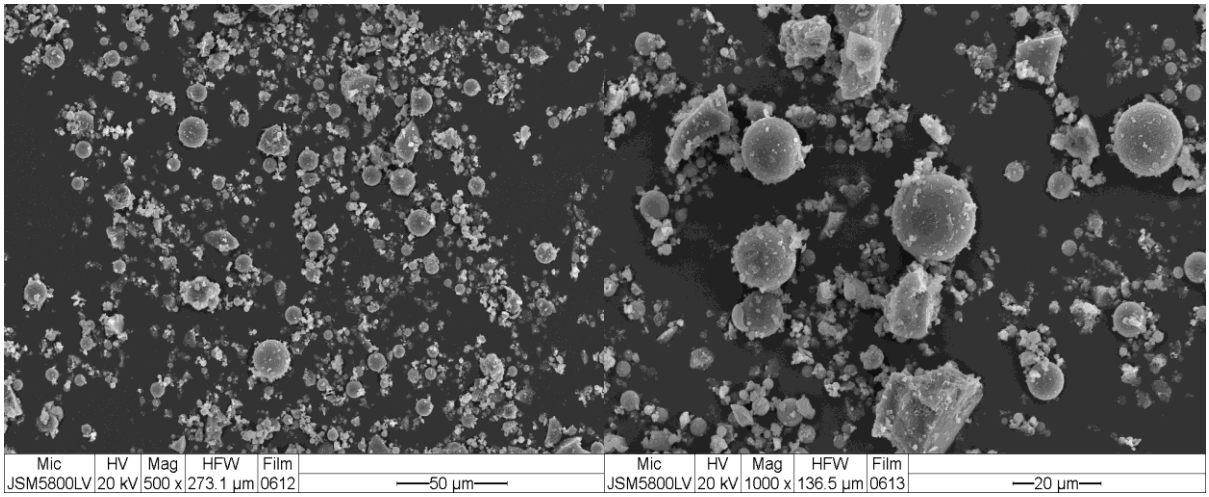


(a) FA 500× (b) FA 1000×

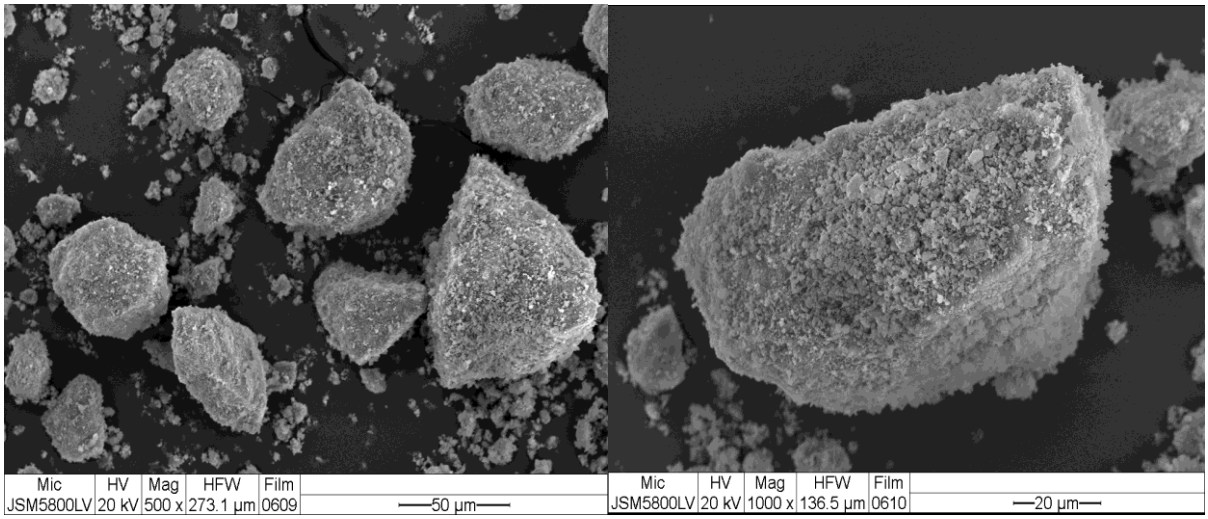


(c) PWA 500× (d) PWA 1000×

**Fig. 3.** SEM image of FA and PWA.

(a) Ash storage (b) Ash disposal

**Fig. 4.** Characteristics of the site.

The alkaline activators used in geopolymerization reactions included sodium silicate ($Na_2SiO_3$) and sodium hydroxide (NaOH). The sodium silicate had a chemical composition of 14.85 wt% NaO, 29.45 wt% $SiO_2$, and 55.70 wt% $H_2O$. The sodium hydroxide was in flake form with 99% purity.

The geopolymer mortars incorporated river sand as the fine aggregate inert component. This sand featured a specific gravity of 2.51 and a maximum particle size of 4.75 mm. According to ASTM C128-18, the water absorption rate of the river sand was measured at 1.48%.

## 2.2 Sample preparation

**Table 2.** Mix proportions of geopolymer mortars with 1,000 g of binder.

| Mix | Binder | | Alkaline | | Sand (g) | Curing |
|---|---|---|---|---|---|---|
| | FA (g) | PWA (g) | SS (g) | SH (g) | | |
| P0H6 | 1,000 | 0 | 571.5 | 228.6 | 2,750 | Hot 6 h |
| P20H6 | 800 | 200 | 571.5 | 228.6 | 2,750 | Hot 6 h |
| P40H6 | 600 | 400 | 571.5 | 228.6 | 2,750 | Hot 6 h |
| P60H6 | 400 | 600 | 571.5 | 228.6 | 2,750 | Hot 6 h |
| P0H12 | 1,000 | 0 | 571.5 | 228.6 | 2,750 | Hot 12 h |
| P20H12 | 800 | 200 | 571.5 | 228.6 | 2,750 | Hot 12 h |
| P40H12 | 600 | 400 | 571.5 | 228.6 | 2,750 | Hot 12 h |
| P60H12 | 400 | 600 | 571.5 | 228.6 | 2,750 | Hot 12 h |
| P0H24 | 1,000 | 0 | 571.5 | 228.6 | 2,750 | Hot 24 h |
| P20H24 | 800 | 200 | 571.5 | 228.6 | 2,750 | Hot 24 h |
| P40H24 | 600 | 400 | 571.5 | 228.6 | 2,750 | Hot 24 h |
| P60H24 | 400 | 600 | 571.5 | 228.6 | 2,750 | Hot 24 h |
| P0A24 | 1,000 | 0 | 571.5 | 228.6 | 2,750 | Ambient 24 h |
| P20A24 | 800 | 200 | 571.5 | 228.6 | 2,750 | Ambient 24 h |
| P40A24 | 600 | 400 | 571.5 | 228.6 | 2,750 | Ambient 24 h |
| P60A24 | 400 | 600 | 571.5 | 228.6 | 2,750 | Ambient 24 h |

SS = sodium silicate, SH = sodium hydroxide

A total of 16 different formulations were created, as detailed in **Table 2**, using binder materials (FA and PWA), sodium silicate, sodium hydroxide, water, and sand aggregate. The study focused on developing geopolymer binders by partially substituting FA with PWA. The experimental design incorporated 16 distinct formulations, representing a full factorial approach for PWA at 20, 40, and 60% by weight, with heat curing at 80°C for 6, 12, and 24 hours, and curing at room temperature for 24 hours. The binder, activator, sand, and water were used in a mass ratio of 1:0.8:2.75:0.25. To prepare the alkali solution, sodium hydroxide flakes were mixed with sodium silicate liquid at a weight ratio of 1:2.5 [23]. The process of preparing the geopolymer mortar consisted of four steps. In Step 1, FA and

PWA were manually blended for approximately 3 minutes. Step 2 involved hand-mixing the binder (FA + PWA) with sand for approximately 3 minutes. In Step 3, NaOH and $Na_2SiO_3$ were blended into a uniform alkaline solution, followed by the addition of water. Step 4 consisted of mixing the binder materials and sand with the alkaline solution. According to Hawa et al. [23], the combination of sodium silicate and sodium hydroxide in Step 3 generates heat, which speeds up the geopolymerization process. Following mixing, the geopolymer slurries were cast into acrylic molds with cube dimensions of 50 mm × 50 mm × 50 mm to set, and produce specimens for compressive strength and compressive strength loss evaluation, compacted according to ASTM C109/C109M-21. Prior to being placed in the oven, the geopolymer mortar molds were completely wrapped in plastic to prevent moisture evaporation from the geopolymer matrix when exposed to the oven heat. The geopolymer mortars were initially cured in acrylic molds at room temperature for 24 hours, followed by heat curing at 80°C for periods of 6, 12, and 24 hours. After demolding, the samples were kept at a consistent ambient temperature of 30 ± 2°C until they were tested. The compressive strength of the geopolymer mortars was evaluated at intervals of 1, 7, and 28 days. Similarly, the compressive strength was tested via seawater immersion. For the microstructural and mineralogical analyses, geopolymer paste specimens were cast in molds measuring 2 cm in diameter and 0.8 cm in thickness. The preparation procedure was identical to that of the geopolymer mortar, except for the sand mixing step.

## 2.3 Characterization techniques

### 2.3.1 Compressive strength and bulk density

The compressive strength tests were performed on cast specimens with dimensions of 50 mm × 50 mm × 50 mm. A universal testing machine specifically designed for mortar was used to carry out these tests. Mortar compressive strength was evaluated according to ASTM C109/C109M-21 at the ages of 1, 7, and 28 days after demolding, with samples cured at ambient temperature. The bulk density of geopolymer mortars was determined at 28 days from their mass-to-volume ratio, using the same specimens after the completion of compressive strength testing.

### 2.3.2 Compressive strength loss

The compressive strength loss after immersion in seawater was measured using cubic cast specimens measuring 50 mm on each side. A universal testing machine specifically designed for mortar was used to perform the tests. The geopolymer samples were tested for strength loss after immersion in seawater for 28 days after demolding.

### 2.3.3 Water absorption

Water absorption tests were conducted to evaluate the actual absorption capacity of geopolymer mortars. Specimens used for this test were cubes measuring 50 mm × 50 mm × 50 mm, cured at ambient temperature for 28 days prior to testing. After curing, samples were immersed in water for durations of 1, 6, 12, and 24 hours. Following immersion, the water absorption values of the geopolymer mortars were calculated according to Eq. (1).

$$(W_b - W_a) \times 100 / W_a \quad (1)$$

$W_a$ = Weight after immersion in water (g)
$W_b$ = Weight before immersion in water (g)

### 2.3.4 Microstructure

The microstructural analysis using SEM imaging was performed to examine the raw materials, geopolymerization products, and pore structures within the geopolymer paste matrices. For the microstructural investigation, only geopolymer pastes containing 0-60% PWA by weight and subjected to curing at ambient temperature were analyzed (specifically samples P0A24, P20A24, P40A24, and P60A24, as detailed in **Table 2**).

### 2.3.5 Mineral analysis

XRD analysis was conducted to identify the crystalline phases present in FA, PWA, and geopolymer pastes. The powdered samples were analyzed with an X'Pert MPD X-ray diffractometer, scanning a 2θ range of 5° to 90° using the clay and rock 0.4 program. The XRD investigation aimed to determine the characteristic crystalline phases and to observe any shifts in peak positions.

#### 2.3.6 Chemical composition

The XRF analysis was employed to determine the chemical compositions of FA, PWA, and geopolymer pastes. This technique was utilized to examine the variations in the chemical compositions of geopolymer pastes resulting from the incorporation of PWA into the binder.

## 3 Results and Discussion

### 3.1 Compressive strength

**Fig. 5** illustrates the compressive strength test results for all mixtures at 1, 7, and 28 days of curing age. The results indicated that all samples with partial replacement of PWA had lower compressive strengths than the samples without PWA (mixtures containing only 100% FA (P0H6, P0H12, and P0H24)) at all aging periods. Notably, three series of samples were heat-cured at 80°C for different durations to evaluate the effect of elevated temperatures on strength development. Interestingly, the specimens without heat curing, containing 20% and 40% PWA, exhibited better compressive strength than the control specimens at both 7 and 28 days of curing. This suggests that heat curing may not always be necessary for achieving optimal strength in PWA-containing mixtures. The compressive strength gain of 100% FA alone was primarily driven by geopolymerization, a process that forms the sodium polysialate (N-A-S-H) gel network [24]. However, the incorporation of PWA at 20%, 40%, and 60% resulted in a gradual reduction in compressive strength across all heat curing conditions. This reduction can partly be attributed to the relatively large particle size of PWA, which leads to reduced reaction efficiency. Additionally, heat curing of geopolymer mortar may induce rapid reactions, causing the alkaline solution to accelerate the reactions within a short period. While this accelerates early-age strength development, it can hinder further strength gains at later ages. The curing temperature plays a crucial role in the formation of geopolymer mortars, as it directly influences the reaction kinetics involved in geopolymerization. Elevated temperatures enhance reaction kinetics, accelerating early-age strength development. However, there exists an optimal temperature range beyond which the increase in strength may level off or even decline [25]. Although geopolymer mixtures cured at higher temperatures achieve greater early-age strength, they do not necessarily lead to significantly higher long-term compressive strength values [26]. These findings align with the study conducted by Hawa [27], which utilized oil palm ash as a precursor material. Hawa's results also indicated that heat curing led to high early-age compressive strength in oil palm ash-based geopolymers. Similarly, the use of fly ash combined with field para rubber latex exhibited a comparable trend in compressive strength development [28, 29]. Overall, the results highlight the importance of balancing heat curing conditions and material composition to optimize both early-age and long-term strength in geopolymer mortars.

**Fig. 5d** illustrates the rise in compressive strength of geopolymer mortar mixtures cured at room temperature with a partial substitution of PWA. The compressive strength of these mortars was influenced by the quantity of PWA incorporated and the duration of curing. In the sample that contained solely PWA, the compressive strength increased from 0.48 MPa after one day of curing to 23.33 MPa after 28 days. According to Abdulkareem et al. [22], the strength progression of P0A24 (100% FA) is primarily influenced by the dissolution and polycondensation processes of the aluminosilicate components in the FA, leading to the formation of a sodium-polysialates (N-A-S-H) gel network, which serves as the binding geopolymeric phase. For samples with 20% and 40% PWA, the compressive strength increased from 0.61 and 0.90 MPa on the first day of curing to 32.31 and 25.48 MPa for 28 days, respectively. Initially, on the first day, all mixtures exhibited similar compressive strengths. However, for 28 days, the specimens displayed different compressive strengths due to variations in the geopolymerization process. The compressive strength of the P60A24 geopolymer exhibited a significant reduction compared to the P0A24 control at 7 and 28 days of curing. Notably, however, P60A24 achieved its peak strength at the 1-day mark, suggesting that high substitution levels of rubber

wood ash (RWA) may promote early-age strength development. This observation aligns with the findings of Abdulkareem et al. [22], who noted that rapid setting times can hinder the formation of a homogeneous and continuous reaction phase, ultimately leading to poor or incomplete polymerization [30]. In the P20A24 sample, which contained 20% PWA and was cured at room temperature, the compressive strength was 0.90 MPa on the first day, and increased to 32.31 MPa at 28 days, with the most notable increase occurring after seven days. It can be observed that the geopolymer incorporating 20% PWA exhibited slow development of early-age compressive strength; however, from 7 to 28 days, the compressive strength increased significantly. This is attributed to the low-temperature curing conditions, which slowed geopolymerization reactions and consequently resulted in lower initial compressive strength. Nevertheless, the compressive strength gradually increased with age as the alkaline solution present in the system slowly reacted over time. This behavior contrasts with heat curing, which accelerates the reaction rate, resulting in higher early-age compressive strength. The presence of CaO as a primary chemical component in PWA plays a significant role in enhancing reactivity, thereby contributing to improved compressive strength development when incorporated in appropriate amounts. This is consistent with the findings of Nuaklong et al. [31], who reported that fly ash geopolymer with high calcium (CaO) content provides higher compressive strength compared to low-calcium fly ash. Overall, the results highlight the importance of balancing PWA content and curing conditions to optimize both early-age and long-term strength in geopolymer mortars.

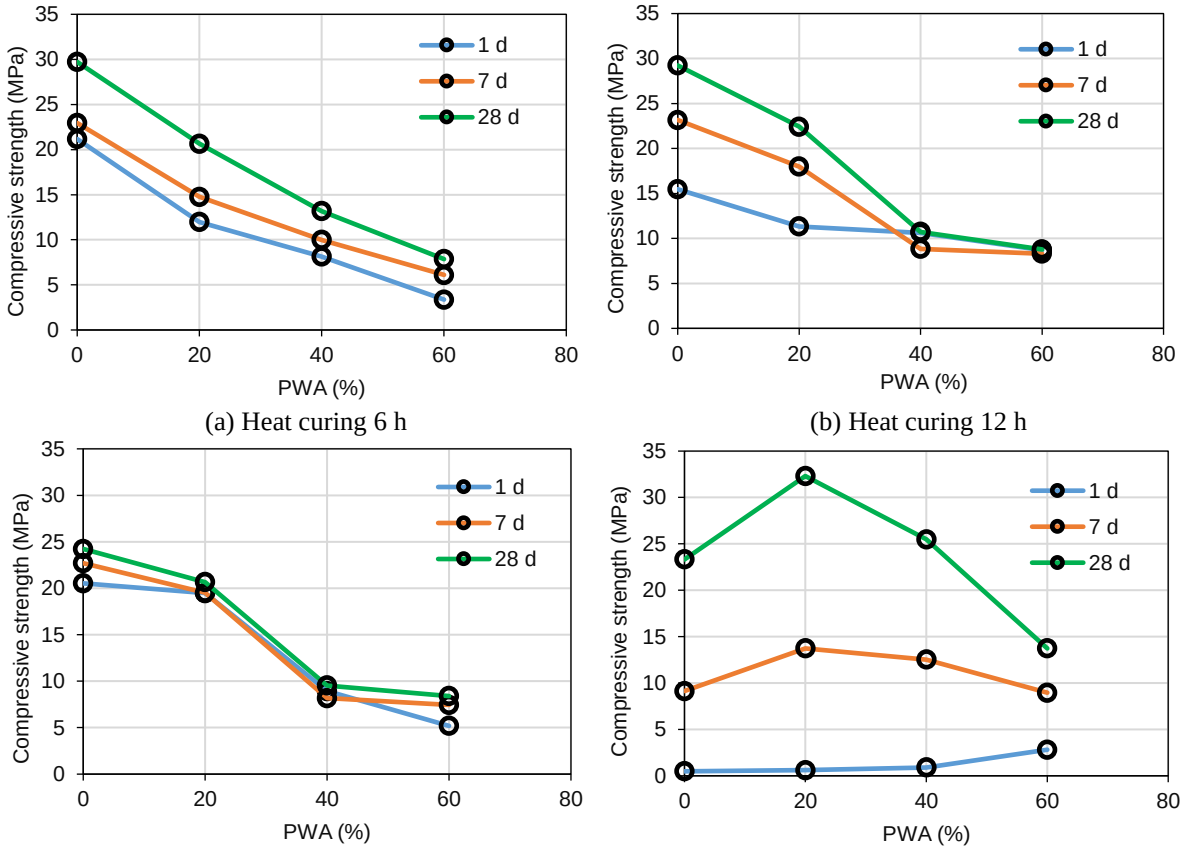


(a) Heat curing 6 h

(b) Heat curing 12 h

(c) Heat curing 24 h

(d) Ambient temperature 24 h

**Fig. 5.** Compressive strength of geopolymer samples under different curing conditions.

### 3.2 Compressive strength loss

**Fig. 6** compares the compressive strength of geopolymer mortar specimens immersed in seawater versus those not immersed in seawater at a curing age of 28 days, for samples subjected to heat curing for 6, 12, and 24 hours. Seawater immersion was conducted immediately after heat curing. After 28 days of seawater immersion, it was observed that the compressive strength of the geopolymer mortar decreased as the proportion of PWA increased across all heat curing durations. Notably, the compressive strength of seawater-immersed specimens showed a slight decline with increasing PWA

content, whereas air-cured geopolymer mortar exhibited a significant reduction in compressive strength with higher PWA content. Additionally, a clear disparity in compressive strength was observed between immersed and non-immersed specimens for geopolymer mortar without PWA and with 20% PWA. However, when the PWA content reached 40% or higher, the compressive strength of geopolymer mortar under both conditions (immersed and non-immersed) became very similar. This suggests that the inclusion of 40% and 60% PWA, combined with heat curing, may lead to rapid setting, resulting in no adverse effects on compressive strength after 28 days of seawater immersion. These findings are supported by the compressive strength test results shown in **Figs. 5a-5c**.

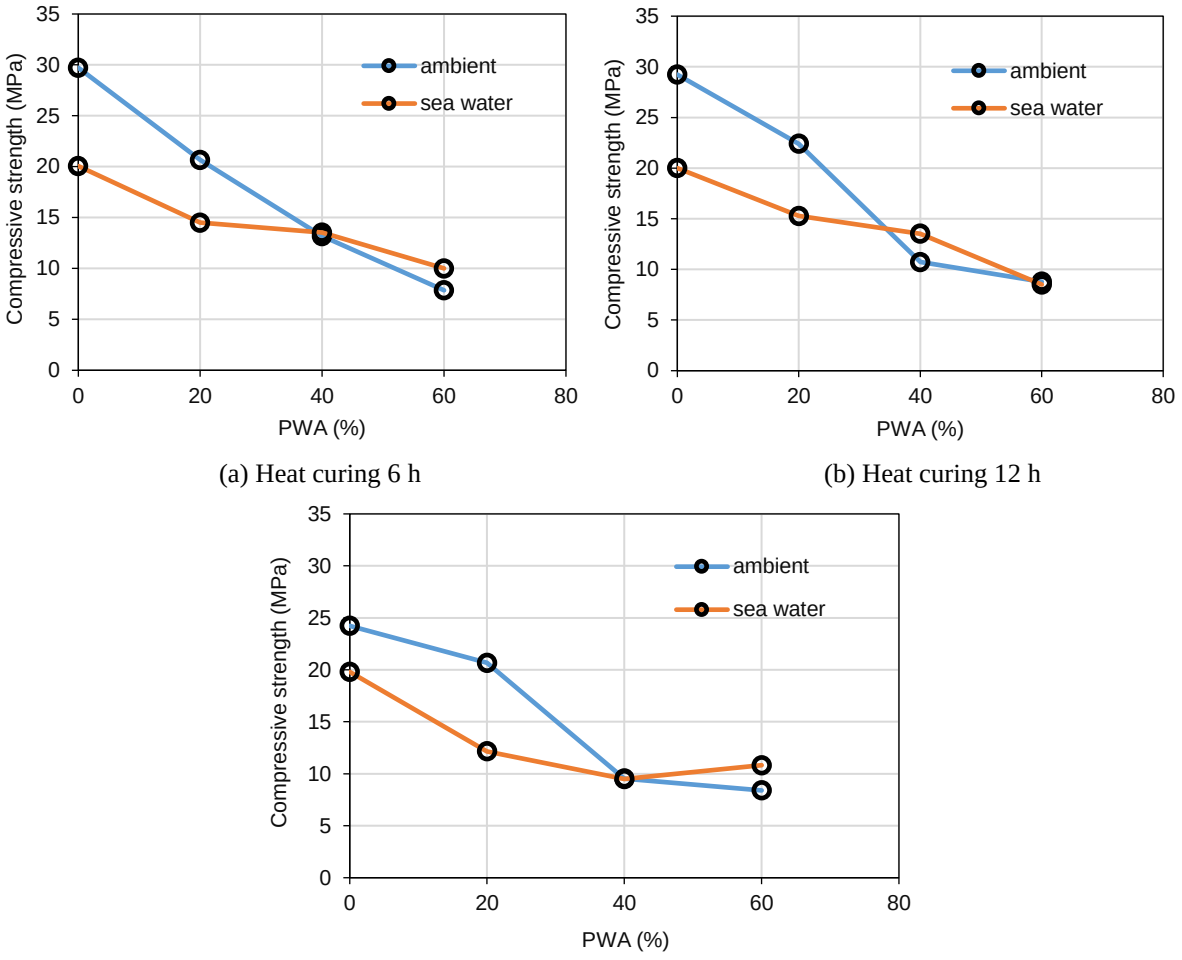


(a) Heat curing 6 h

(b) Heat curing 12 h

(c) Heat curing 24 h

**Fig. 6.** Compressive strength of geopolymer samples under different curing conditions at 28 days.

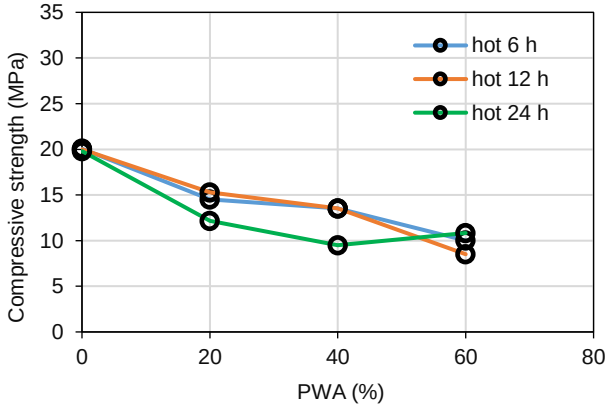


**Fig. 7.** Compressive strength of geopolymer samples immersed in seawater at 28 days.

**Fig. 7** compares the compressive strength of geopolymer mortar immersed in seawater after heat curing for 6, 12, and 24 hours. It is evident that the compressive strength decreases as the PWA content increases across all heat curing durations. For specimens subjected to 6 and 12 hours of heat curing, the compressive strength values show only minor differences for all mix ratios. This suggests that the difference in heat curing duration of 6 hours has a minimal effect on the compressive strength. The percentage loss in compressive strength for seawater-immersed specimens compared to non-immersed specimens ranges between 29.77 to 32.5%. When considering specimens without PWA, the compressive strengths across the three heat curing durations are very similar, with values of 20.06, 20.00, and 19.8 MPa for 6, 12, and 24 hours of heat curing, respectively.

### 3.3 Water absorption

Evaluating water absorption is essential for determining the durability and effectiveness of geopolymer materials. This research involved a water absorption test to analyze how geopolymerization influences the pore structure of geopolymer matrices composed of FA and PWA. The study specifically focused on how substituting PWA affects the water absorption characteristics of geopolymer mortars. Tests were conducted after 7 and 28 days of curing under two conditions: heat curing at high temperatures and ambient curing at room temperature. As shown in **Fig. 8**, the water absorption of all mixtures exhibited slight but consistent changes, ranging from 7.47% to 10.53% across all tested ages. This range indicates that replacing PWA has a noticeable yet moderate effect on water absorption properties.

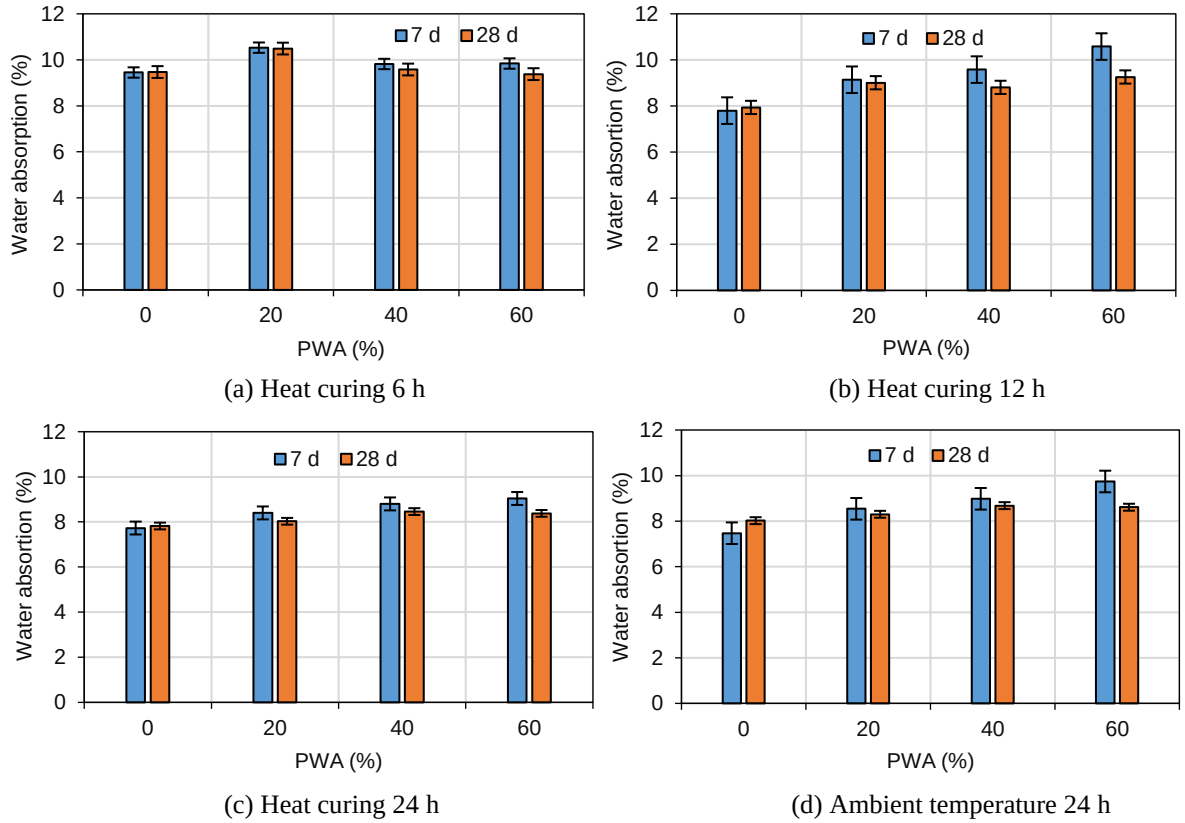


(a) Heat curing 6 h

(b) Heat curing 12 h

(c) Heat curing 24 h

(d) Ambient temperature 24 h

**Fig. 8.** Water absorption of geopolymer mortars at 28 days.

The least water absorption was observed in the control mixture without PWA inclusion across all curing conditions. From the results, it was noted that the water absorption of geopolymers containing PWA tended to increase compared to the sample without PWA, particularly in heat-cured geopolymers. This increase in water absorption can be attributed to the larger average particle size of PWA compared to fly ash. The larger particles of PWA were unable to fill the voids in the geopolymer matrix effectively, leading to a less dense microstructure. Furthermore, the larger particle size of PWA hindered its active participation in the geopolymerization process. As a result, insufficient reaction products were formed

to fill the voids, which contributed to higher water absorption. This observation aligns with the findings of Asante et al. [32], who reported that unground fly ash (with larger particle sizes) results in higher water absorption compared to ground fly ash (with smaller particle sizes). Their study emphasized that larger particles cannot pack tightly within the composite material, leaving more voids and increasing water absorption.

Upon examining geopolymers cured for both 7 and 28 days, it was observed that the water absorption percentage experienced a slight reduction at the 28-day mark. This reduction is likely due to the enhanced geopolymerization reaction of fly ash over time. Nevertheless, the decrease in water absorption percentage across all mix ratios was limited to a maximum of 1.32%, suggesting that the inclusion of PWA in the geopolymer did not significantly elevate its water absorption. The test results align with the findings of Gill et al. [33] from their investigation into the water absorption of fly ash-based geopolymer mixed with marble powder.

### 3.4 Bulk density

**Fig. 9** presents the densities of geopolymer mortars subjected to both heat curing and room-temperature curing conditions. It was evident that the density of these mortars diminished with extended heat curing. For instance, in the geopolymer mortar containing 20% PWA, the densities for samples P20A24, P20H6, P20H12, and P20H24 were recorded as 2146, 2133, 2118, and 2103 kg/m³, respectively. This decline is due to the prolonged hot curing, which reduces water content as it is consumed during the reaction process. Additionally, extended heat curing led to partial water evaporation from the geopolymer matrix, which then condensed on the plastic mold wrapping. When left at room temperature for up to 28 days, further evaporation took place. Moreover, the larger particle size of PWA created larger voids, making evaporation easier. This aligns with the water absorption test results, which indicate that as the PWA content increases, water absorption also rises.

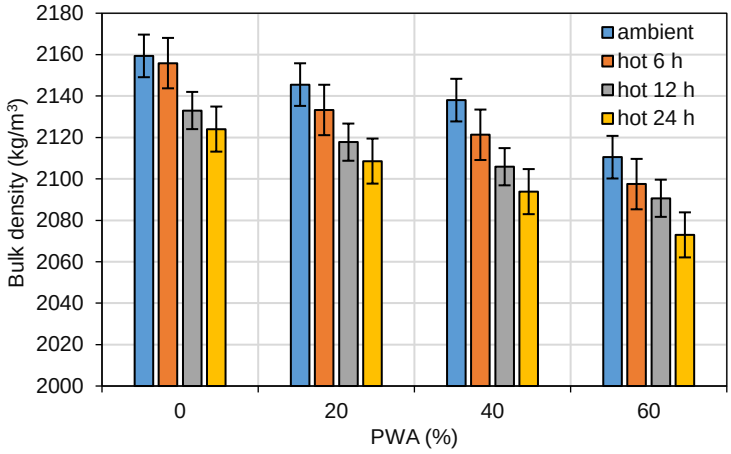


**Fig. 9.** Density of geopolymer samples at 28 days.

### 3.5 SEM

SEM micrographs of geopolymer paste at different PWA content levels with an ambient temperature curing condition at the age of 28 days are shown in **Fig. 10**. The micrograph of the P0A24 sample shows a heterogeneous and porous matrix with the appearance of agglomerated precipitation products connected together, as well as many small microcracks. Abdulkareem et al. [22] reported that minor microcracks form due to the loss of free water through evaporation throughout the curing and aging stages. It is noteworthy that a small number of unreacted fly ash (FA) spherical particles were observed. This suggests the possibility that the high volume of alkaline solution in this mix promoted the complete dissolution of the FA particles. However, numerous small microcracks were found extensively distributed throughout the matrix.

The effects of the partial substitution of FA with PWA on the microstructure and mechanical properties of geopolymer mortars were investigated. The addition of PWA at 20% (P20A24) and 40%

(P40A24) of the total binder content significantly improved the microstructure compared to the control mixture (P0A24). SEM images at 28 days (**Figs. 10b** and **10c**) reveal enhanced uniformity and density in the gel matrix for both mixtures, particularly for P20A24. Notably, fly ash microspheres were entirely absent in these mixtures, indicating that the highly alkaline environment created by PWA facilitated complete FA dissolution. The resulting reaction products contributed to refining the microstructure and reducing microcracks [34]. The P20A24 mixture exhibited superior mechanical properties due to its densely reacted geopolymer matrix and minimal microcracking. While P40A24 also showed reduced microcracks compared to the control, it developed significant porosity that weakened its compressive strength relative to P20A24. Nevertheless, both mixtures outperformed the control (P0A24) in terms of structural integrity. In contrast, the microstructure of the P60A24 mixture (**Fig. 10d**) displayed a poorly reacted matrix with a loose and clumped texture. This inefficiency in geopolymerization was likely caused by excessive FA substitution with PWA at 60%, which led to an overproduction of sodium-related compounds during precursor dissolution. XRD analysis (**Fig. 11**) confirmed the presence of thermonatrite in this mixture, a phase known to negatively affect geopolymer strength. Overall, these findings suggest that moderate substitution levels of FA with PWA (up to 40%) can enhance both microstructural characteristics and mechanical performance. However, excessive substitution levels (e.g., 60%) result in diminished performance due to poor reaction efficiency and increased porosity.

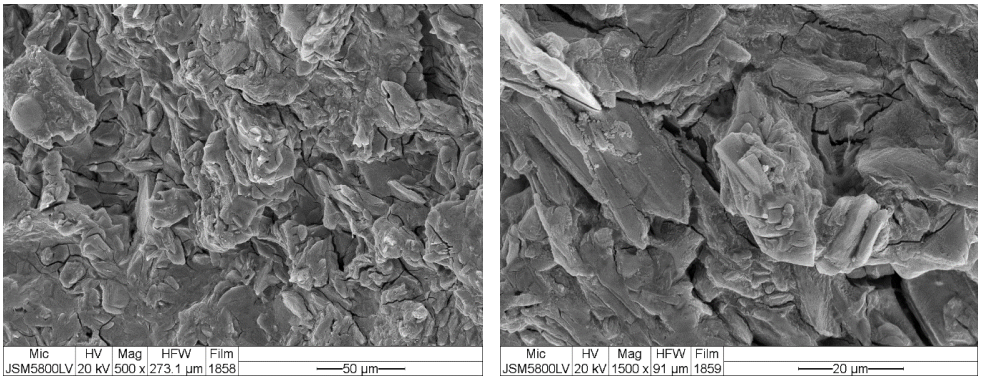


(a) P0A24, 500× and 1,500×

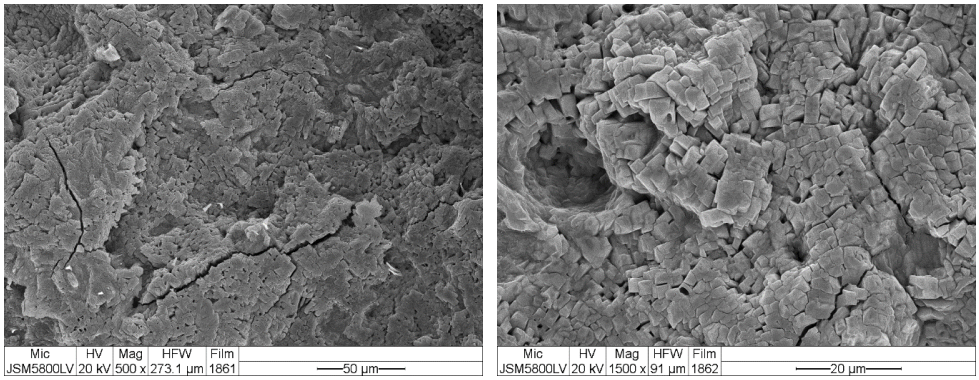


(b) P20A24, 500× and 1,500×

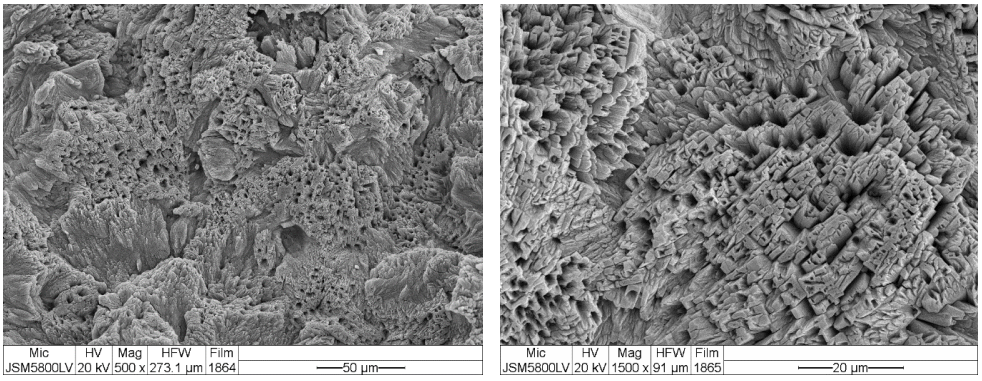


(c) P40A24, 500× and 1,500×

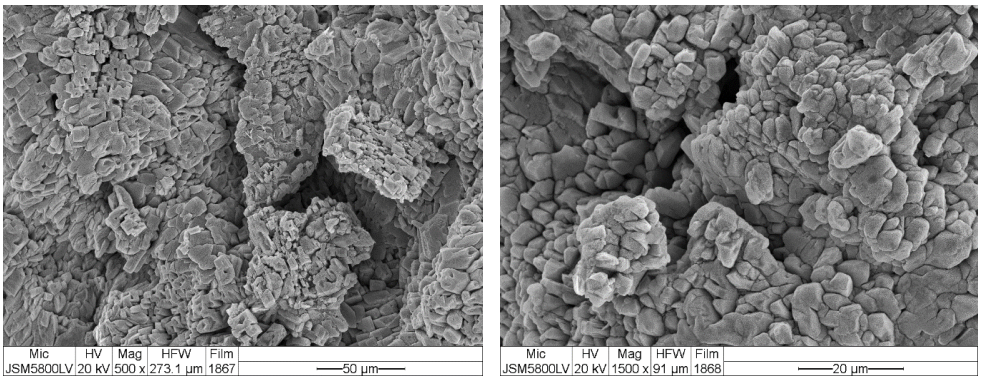


(d) P60A24, 500× and 1,500×

**Fig. 10.** SEM images of geopolymer paste 500× and 1,500×.

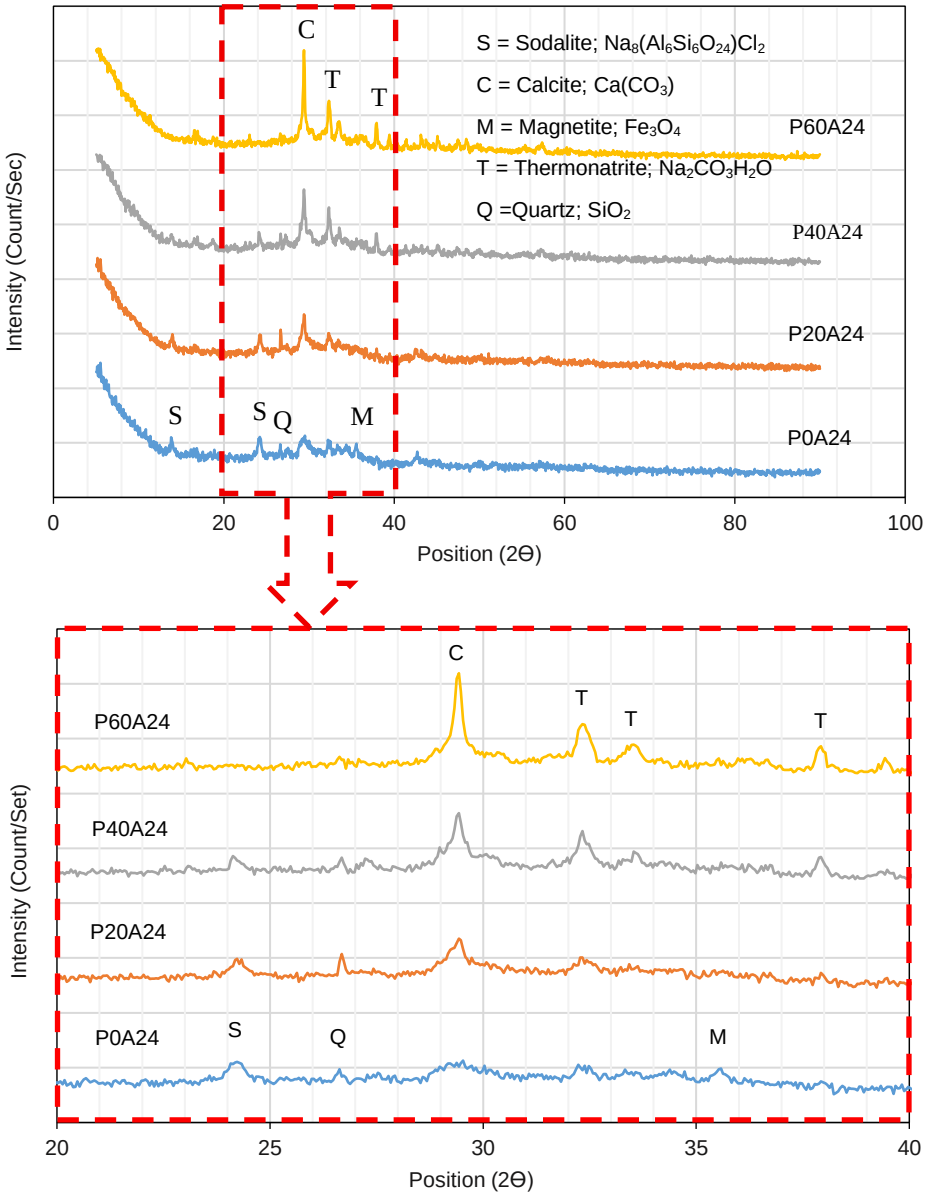


**Fig. 11.** XRD pattern of geopolymer pastes after curing at ambient temperature.

### 3.6 X-ray diffraction analysis

**Fig. 11** presents the XRD analysis of the resulting geopolymer pastes, which was conducted to investigate the phase composition and structural changes after geopolymerization. All mixtures exhibited a characteristic high background between 20° and 38° 2θ, indicative of the presence of amorphous phases, along with increased crystalline peaks associated with the base materials. Notably, the high background shifted from 21° and 39° 2θ for the P0A24 sample and from 25° and 40° 2θ for P60A24 in the initial materials to 20° and 38° 2θ after geopolymerization. The observed shift indicates the development of an amorphous sodium aluminosilicate hydrate (N-A-S-H) gel along with a three-dimensional structural network [35]. As Abdulkareem et al. [22] reported, a broad hump in the XRD pattern is typically an indicator of an amorphous component, implying a high degree of geopolymerization and the formation of a significant quantity of amorphous geopolymeric products. In addition to the amorphous phase, the P0A24 sample (without PWA) displayed some partially crystalline traces, which were originally detected in the fly ash (FA), as well as a newly formed phase of sodalite (sodium aluminum silicate chloride; $Na_8(Al_6Si_6O_{24})Cl_2$) resulting from the geopolymerization. The formation of sodalite is noteworthy, as Ulian and Valdrè [36] identified it as an important mineral belonging to the zeolite group, which may influence the properties and performance of the resulting geopolymer material. Wang et al. [37] reported that the N-A-S-H framework in geopolymers with an n(Si)/n(Al) ratio of 1 closely resembles the structure of sodalite. Consequently, the detection of sodalite through XRD analysis serves as a vital confirmation of N-A-S-H gel formation within the matrix.

The XRD patterns of samples P20A24, P40A24, and P60A24 revealed notable variations in crystalline composition compared to the control sample, highlighting the impact of increasing PWA content. Specifically, the intensity of the main sodalite peaks at approximately 14° and 24° 2θ decreased as the PWA content increased, a trend attributed to the dilution of fly ash (FA) in the geopolymer mixtures. In parallel, a new sodium-based phase, thermonatrite ($Na_2CO_3 \cdot H_2O$), became increasingly prominent with higher PWA content. Furthermore, a distinct increase in the intensity of calcite peaks at approximately 30° (2Θ) was observed with high volume of PWA. According to Chindaprasirt et al. [38], the diffraction peak at 30° represents the C-A-S-H phase. The formation of C-A-S-H typically enhances the mechanical performance of geopolymers. However, excessive PWA incorporation led to the prominent formation of thermonatrite. This suggests the presence of excess sodium (from the NaOH or $Na_2SiO_3$ activators) that failed to integrate into the aluminosilicate framework for N-A-S-H gel synthesis. This 'free' sodium subsequently migrates to the surface, reacts with atmospheric $CO_2$, and crystallizes, which is an indication that the activator dosage exceeded the absorption capacity of the precursors. This phenomenon is likely a contributing factor to the degradation of compressive strength. Perez-Cortes et al. [39] reported that thermonatrite dissolves during fresh binder mixing, which enhances the system's alkalinity. This elevated alkalinity promotes the dissolution of aluminosilicate precursors and supplies additional $Na^+$ ions, thereby creating an environment favorable for (N,C)-A-S-H gel formation [40]. However, the prominent detection of thermonatrite in the 60% PWA-blended geopolymer sample suggests that the reaction was incomplete, leaving a substantial amount of residual sodium carbonate. This excess unreacted sodium carbonate, in turn, adversely affects the development of compressive strength.

### 3.7 XRF

The purpose of this analysis is to investigate how the incorporation of parawood ash affects the chemical composition and compressive strength of air-cured geopolymer pastes. **Table 3** and **Fig. 12** present the XRF chemical composition analysis results for these pastes. The data show that as the proportion of parawood ash in the mixture increases, the contents of $SiO_2$ and $Al_2O_3$ decrease, while those of CaO and $K_2O$ increase. This trend is expected, given that parawood ash is primarily composed of CaO and $K_2O$ and contains relatively low amounts of $SiO_2$ and $Al_2O_3$. In contrast, the $Na_2O$ content remains relatively stable, owing to the constant alkaline activator ratio used in all mixtures. In geopolymer research, particular attention is paid to the $SiO_2/Al_2O_3$ ratio, as it significantly influences compressive strength. Previous studies, such as that by Chindaprasirt et al. [41], have shown that a fly ash-based geopolymer blended with iron slag at a $SiO_2/Al_2O_3$ molar ratio of 4.79 achieved a compressive strength of 30.9 MPa, which is comparable to the strength observed in sample P20A24 ($SiO_2/Al_2O_3 = 3.34$) in the present study. Here, the $SiO_2/Al_2O_3$ ratio was determined via XRF analysis of the geopolymer paste after the reaction. The results indicate that a $SiO_2/Al_2O_3$ ratio of 3.34 (P20A24)

yields the highest compressive strength, while samples with ratios of 3.29 (P0A24) and 4.03 (P40A24) exhibit lower strengths. Furthermore, when the $SiO_2/Al_2O_3$ ratio increases to 4.92 (P60A24), the compressive strength decreases significantly (see **Fig. 5d**). These findings underscore the importance of optimizing the $SiO_2/Al_2O_3$ ratio to achieve maximum compressive strength in geopolymer pastes.

**Table 3.** The chemical composition of geopolymer pastes after curing at ambient temperature.

| Oxide | Content (% weight) | | | |
|---|---|---|---|---|
| | P0A24 | P20A24 | P40A24 | P60A24 |
| $SiO_2$ | 34.28 | 29.17 | 25.61 | 21.36 |
| $Al_2O_3$ | 10.41 | 8.74 | 6.36 | 4.34 |
| $Fe_2O_3$ | 10.26 | 8.4 | 5.88 | 4.17 |
| CaO | 13.28 | 16.51 | 17.69 | 20.65 |
| $K_2O$ | 1.79 | 2.68 | 3.28 | 4.1 |
| $SO_3$ | 1.76 | 1.5 | 1.24 | 1.1 |
| MgO | 1.35 | 1.99 | 2.4 | 2.71 |
| $P_2O_5$ | 0.25 | 0.47 | 0.78 | 1.08 |
| MnO | 0.12 | 0.18 | 0.26 | 0.32 |
| SrO | 0.1 | 0.1 | 0.09 | 0.1 |
| $TiO_2$ | 0.31 | 0.28 | 0.2 | 0.15 |
| $Na_2O$ | 17.06 | 16.74 | 18.58 | 17.3 |
| Cl | | | 0.1 | 0.1 |
| $Rb_2O$ | | | | 0.04 |
| Oxide ratio | | | | |
| $SiO_2/Al_2O_3$ | 3.29 | 3.34 | 4.03 | 4.92 |
| $CaO/SiO_2$ | 0.39 | 0.57 | 0.69 | 0.97 |
| $CaO/Al_2O_3$ | 1.28 | 1.89 | 2.78 | 4.76 |

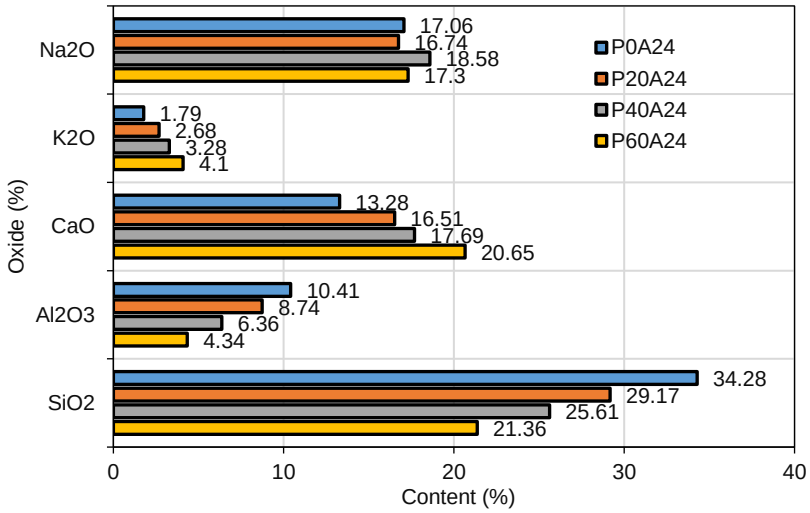


**Fig. 12.** The main chemical composition of geopolymer pastes.

**Fig. 13** presents the XRF analysis results for the $SiO_2/Al_2O_3$, $CaO/SiO_2$, and $CaO/Al_2O_3$ ratios in the samples, compared with their initial molar ratios, to assess the changes resulting from geopolymerization. The results show that although the XRF-determined ratios are consistently lower than the initial molar ratios, there is a strong correlation between the two sets, as indicated by the high $R^2$ values for all three ratios. For example, as shown in **Fig. 13a**, the $SiO_2/Al_2O_3$ ratios of samples P0A24, P20A24, P40A24, and P60A24 were 3.29, 3.34, 4.03, and 4.92, respectively, and significantly lower than their corresponding initial molar ratios of 4.59, 4.96, 5.56, and 6.70. This consistent reduction suggests that after geopolymerization, the original chemical constitution of the raw materials was modified through alkaline dissolution and the subsequent generation of novel reaction compounds, which directly affected the percentages of $SiO_2$, $Al_2O_3$, and other constituents. The importance of the $SiO_2/Al_2O_3$ ratio is further supported by Juengsuwattananon et al. [42], who reported that maximum strength was achieved at an initial $SiO_2/Al_2O_3$ molar ratio of 4.0. However, when the ratio increased to 6.0–7.0, sodium bicarbonate compounds and unreacted raw materials were observed, indicating

incomplete reaction efficiency. These findings highlight the need to carefully control the $SiO_2/Al_2O_3$ ratio to optimize the performance of geopolymer materials.

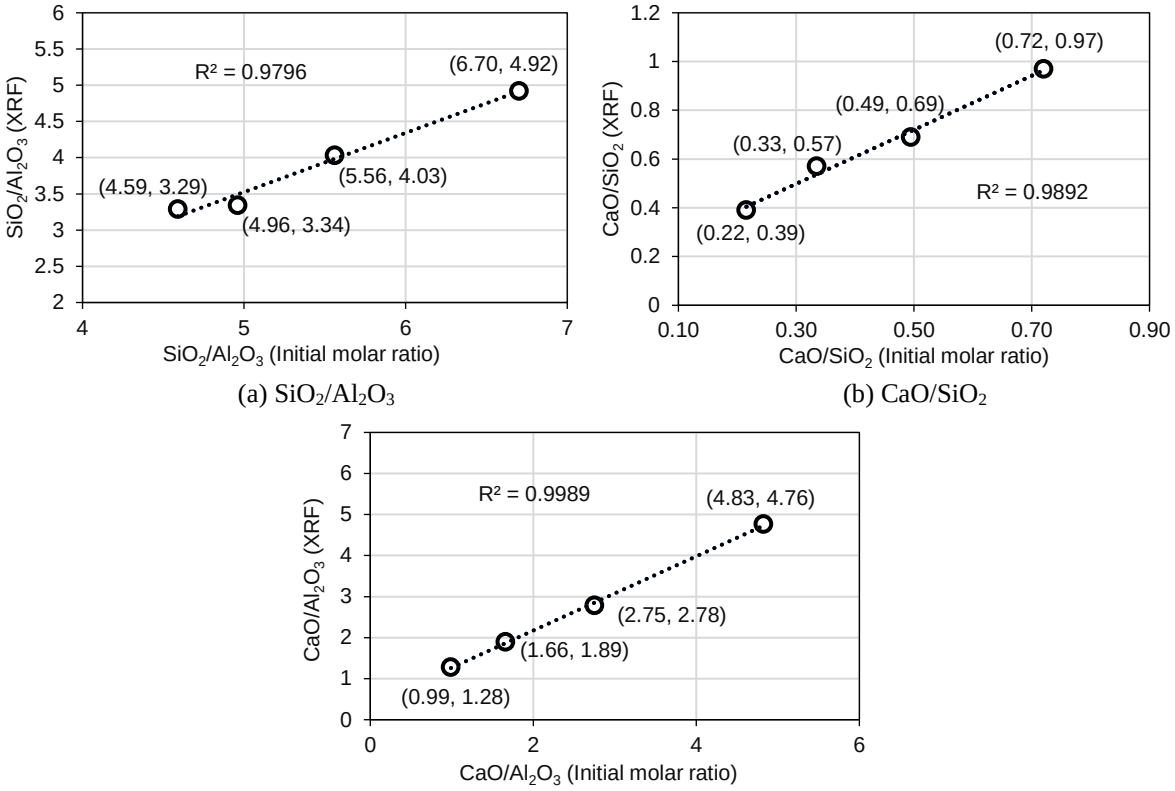


(a) $SiO_2/Al_2O_3$ (b) $CaO/SiO_2$

(c) $CaO/Al_2O_3$

**Fig. 13.** Relationship of initial molar ratio and product ratio.

## 4 Conclusions

This study investigated the effects of parawood ash (PWA) and curing conditions on the compressive strength, durability, and microstructures of fly ash-based geopolymers. The conclusions were summarized as follows:

- Partial replacement of fly ash (FA) with PWA generally reduced compressive strength, but samples with 20% and 40% PWA cured at ambient temperature showed significant strength gains at later ages, sometimes surpassing heat-cured controls.
- Heat curing accelerates early strength development but may limit long-term strength, while ambient curing allows for gradual strength increase, especially in mixtures with optimal PWA content.
- The results emphasize the need to balance PWA content and curing conditions to achieve optimal early-age and long-term compressive strength in geopolymer mortars.
- Increasing PWA content leads to decreased compressive strength in both seawater-immersed and air-cured geopolymer mortars, with the reduction being more pronounced in air-cured samples; at 40% or higher PWA, compressive strengths of immersed and non-immersed specimens become similar.
- The duration of heat curing (6, 12, or 24 hours) has minimal effect on compressive strength, while seawater immersion results in a 29.77–32.5% strength loss compared to non-immersed specimens.
- Substituting PWA for fly ash in geopolymer mortars moderately increases water absorption, especially in heat-cured samples, due to the larger particle size of PWA leading to a less dense microstructure.
- Water absorption slightly decreases from 7 to 28 days due to ongoing geopolymerization, but the overall increase from PWA inclusion remains limited, indicating no significant negative impact on durability.

- Prolonged heat curing and higher PWA content reduce the density of geopolymer mortars by increasing water loss and void formation, as confirmed by both density and water absorption test results.
- Moderate substitution of fly ash with PWA (up to 40%) improves the microstructure and mechanical properties of geopolymer mortars, while excessive substitution (60%) leads to poor reaction efficiency, increased porosity, and reduced strength.
- XRD analysis shows that moderate PWA substitution in geopolymer pastes promotes amorphous gel formation and structural refinement, while high PWA content leads to increased thermonatrite and residual sodium carbonate, resulting in incomplete reactions and reduced compressive strength.
- Increasing parawood ash content in air-cured geopolymer pastes alters the chemical composition, lowering $SiO_2$ and $Al_2O_3$ while raising CaO and $K_2O$, and demonstrates that an optimal $SiO_2/Al_2O_3$ ratio (around 3.34) maximizes compressive strength, highlighting the need for careful ratio optimization.
- XRF analysis reveals that geopolymerization lowers the $SiO_2/Al_2O_3$, $CaO/SiO_2$, and $CaO/Al_2O_3$ ratios compared to initial values, emphasizing the importance of optimizing the $SiO_2/Al_2O_3$ ratio to achieve maximum strength and efficient reactions in geopolymer materials.

## Acknowledgement

The authors would like to express their gratitude to the Infrastructure and Materials Innovation Research Unit and the Department of Civil Engineering at the Faculty of Engineering, Princess of Naradhiwas University, located in Amphur Muang, Narathiwat, for generously providing access to their facilities.

## CRediT authorship contribution statement

**Abideng Hawa:** Investigation, Formal analysis, Conceptualization, Supervision, Writing – original draft. **Preecha Saleamea:** Conceptualization, Formal analysis. **Woraphot Prachasaree:** Writing – review & editing.

## Conflicts of interest

The authors declare that they have no conflicts of interest to report regarding the present study.

## Data availability statement

The data presented in this study are available on request from the corresponding author.

## References

[1] World Bioenergy Association, GLOBAL BIOENERGY STATISTICS 2023, https://www.worldbioenergy.org/uploads/231219%20GBS%20Report.pdf, 2023 (accessed Marh 6, 2025).
[2] Department of Alternative Energy Development and Efficiency (DEDE), Ministry of Energy. https://kc.dede.go.th/knowledge-view-file.aspx?p=213,2024 (accessed April 9, 2026).
[3] Khodr M, Law DW, Gunasekara C, Setunge S, Brkljaca R. Compressive strength and microstructure evolution of low calcium brown coal fly ash-based geopolymer. Journal of Sustainable Cement-Based Materials 2020; 9(1): 17-34. https://doi.org/10.1080/21650373.2019.1666061.
[4] Shams H, Hayat S, Ullah H, Abdrhman H, Qiu Y. Alkali-Silica potential in fly-ash-based geopolymer concrete. Materials and Structures 2024; 57: 192. https://doi.org/10.1617/s11527-024-02479-8.
[5] Paramban RK, Govindarajulu KV. Characteristic study of geopolymer fly ash fine aggregate and its influence on partial replacement of M-sand in the strength properties of mortar. Structures 2024; 68: 107141. https://doi.org/10.1016/j.istruc.2024.107141.
[6] Ariyadasa PW, Manalo AC, Lokuge W, Aravinthan V, Pasupathy K, Gerdes A. Bond performance of fly ash-based geopolymer mortar in simulated concrete sewer substrate. Construction and Building Materials 2024; 446: 137927. https://doi.org/10.1016/j.conbuildmat.2024.137927.
[7] Mohana R, Bharathi SML. Assessment on the mesh and mortar effect of the impact resistant nano fly ash based geopolymer ferrocement panels using rubber and plastic aggregates. Structures 2024; 68: 107147. https://doi.org/10.1016/j.istruc.2024.107147.

[8] Huang Z, Zhou Y, Salahuddin H. Development and performance evaluation of sustainable lightweight geopolymer based fireproofing coatings for steel construction. Sustainable Structures 2024; 4(2): 00044. https://doi.org/10.54113/j.sust.2024.000044.
[9] Kumar BG, Selvam R, Govindaraj V. Durability assessment of blended slag-fly ash geopolymer concrete in field conditions after 5 years. Journal of Sustainable Cement-Based Materials 2024; 13(12): 1770-1781. https://doi.org/10.1080/21650373.2024.2409937.
[10] Duan P, Yan C, Zhou W. Influence of partial replacement of fly ash by metakaolin on mechanical properties and microstructure of fly ash geopolymer paste exposed to sulfate attack. Ceramics International 2016; 42(2): part B, 3504-3517. https://doi.org/10.1016/j.ceramint.2015.10.154.
[11] Ashfaq MH, Sharif MB, Irfan-ul-Hassan M, Sahar U, Akmal U, Mohamed A. Up-scaling of fly ash-based geopolymer concrete to investigate the binary effect of locally available metakaolin with fly ash. Heliyon, 2024; 10(4): e26331. https://doi.org/10.1016/j.heliyon.2024.e26331.
[12] Al-Naghi AAA, Ghazouani N, Selmi A, Alashker Y, Raza A. Combined effects of elevated temperature, sulfates and chlorides on performance of fly ash and metakaolin-based recycled aggregate geopolymer concrete. Journal of Building Engineering 2025; 99: 111561. https://doi.org/10.1016/j.jobe. 2024.111561.
[13] Nadziri N, Ismail I, Hamdan S. Binding gel characterization of alkali-activated binders based on palm oil fuel ash (POFA) and fly ash. Journal of Sustainable Cement-Based Materials 2018; 7(1): 1-14. https://doi.org/10.1080/21650373.2017.1299054.
[14] Ranjbar N, Mehrali M, Alengaram UJ, Metselaar HSC, Jumaat MZ. Compressive strength and microstructural analysis of fly ash/palm oil fuel ash based geopolymer mortar under elevated temperatures. Construction and Building Materials 2014; 65: 114-121. https://doi.org/10.1016/j.conbuildmat.2014.04.064.
[15] Poltue T, Suddeepong A, Horpibulsuk S, Samingthong W, Arulrajah A, Rashid ASA. Strength development of recycled concrete aggregate stabilized with fly ash-rice husk ash based geopolymer as pavement base material. Road Materials and Pavement Design 2020; 21(8): 2344-2355. https://doi.org/10.1080/14680629.2019.1593884.
[16] Somna R, Saowapun T, Somna K, Chindaprasirt P. Rice husk ash and fly ash geopolymer hollow block based on NaOH activated. Case Studies in Construction Materials 2022; 16: e01092. https://doi.org/10.1016/j.cscm.2022.e01092.
[17] Zhu H, Liang G, Xu J, Wu Q, Zhai M. Influence of rice husk ash on the waterproof properties of ultrafine fly ash based geopolymer. Construction and Building Materials 2019; 208: 394-401. https://doi.org/10.1016/j.conbuildmat.2019.03.035.
[18] Rihan MAM, Onchiri RO, Gathimba N, Sabuni B. Assessing the durability performance of geopolymer concrete utilizing fly ash and sugarcane bagasse ash as sustainable binders. Open Ceramics 2024; 20: 100687. https://doi.org/10.1016/j.oceram.2024.100687.
[19] Chuewangkam N, Nachaithong T, Chanlek N, Thongbai P, Pinitsoontorn S. Mechanical and dielectric properties of fly ash geopolymer/sugarcane bagasse ash composites. Polymers 2022; 14(6): 1140. https://doi.org/10.3390/polym14061140.
[20] Ates F, Park KT, Kim KW, Woo BH, Kim HG. Effects of treated biomass wood fly ash as a partial substitute for fly ash in a geopolymer mortar system. Construction and Building Materials 2023; 376: 131063. https://doi.org/10.1016/j.conbuild mat.2023.131063.
[21] Catauro M, Viola V, D'Amore A. Filling fresh metakaolin-based geopolymer paste with wood ash: chemical and mechanical characterization. Macromolecular Symposia 2024; 413(4): 2300252. https://doi.org/10.1002/masy.202300252.
[22] Abdulkareem OA, Ramli M, Matthews JC. Production of geopolymer mortar system containing high calcium biomass wood ash as a partial substitution to fly ash: an early age evaluation. Composites Part B: Engineering 2019; 174: 106941. https://doi.org/10. 1016/j.compositesb.2019.106941.
[23] Hawa A, Tonnayopas D, Prachasaree W, Taneerananon P. Development and performance evaluation of very high early strength geopolymer for rapid road repair. Advances in Materials Science and Engineering 2013; 764180. https://doi.org/10.1155/2013/764180.
[24] Provis JL, Bernal SA. 2014. Geopolymers and related alkali-activated materials. Annual Review of Materials Research 2014; 44: 299-327. https://doi.org/10.1146/annurev-matsci-070813-113515.
[25] Zhang Y, Xiao R, Jiang X, Li W, Zhu X, Huang B. Effect of particle size and curing temperature on mechanical and microstructural properties of waste glass-slag-based and waste glass-fly ash-based geopolymers. Journal of Cleaner Production 2020; 273: 122970. https://doi.org/10.1016/j.jclepro.2020.122970.
[26] Mijarsh MJA, Johari MAM, Ahmad ZA. Effect of delay time and $Na_2SiO_3$ concentrations on compressive strength development of geopolymer mortar synthesized from TPOFA. Construction and Building Materials 2015; 86: 64-74. https://doi.org/10.1016/ j.conbuildmat.2015.03.078.
[27] Hawa A. Strength and microstructural of geopolymer mortar from palm oil ash containing alumina powder with palm oil clinker aggregate. Engineering and Applied Science Research 2022; 49(6): 731-743. https://d

oi.org/10.14456/easr.2022.71.
[28] Hawa A, Salaemae P, Prachasaree W, Tonnayopas D. Compressive strength and microstructural characteristics of fly ash based geopolymer with high volume field Para rubber latex. Romanian journal of materials 2017; 47(4): 462-469.
[29] Hawa A,Salaemae P, Prachasaree W. The development of compressive strength, drying shrinkage and microstructure of fly ash geopolymer with field Para rubber latex. Romanian journal of materials 2020; 50(1): 59-68.
[30] Rajamma R, Ferreira VM, Labrincha JA. Alkali activation of biomass fly ash–metakaolin blends. Fuel 2012; 98: 265-271. https://doi.org/10.1016/j.fuel.2012.04.006.
[31] Nuaklong P, Wongsa A, Sata V, Boonserm K, Sanjayan J, Chindaprasirt P. Properties of high-calcium and low-calcium fly ash combination geopolymer mortar containing recycled aggregate. Heliyon 2019; 5(9): e02513. https://doi.org/10.1016/j.heliyon.2019. e02513.
[32] Asante B, Schmidt G, Teixeira R, Krause A, Junior HS. Influence of wood pretreatment and fly ash particle size on the performance of geopolymer wood composite. European Journal of Wood and Wood Products 2021; 79: 597–609. https://doi.org/10.1007/s00107-021-01671-9.
[33] Gill P, Rathanasalam VS, Jangra P, Pham TM, Ashish DK. Mechanical and microstructural properties of fly ash-based engineered geopolymer mortar incorporating waste marble powder. Energy, Ecology and Environment 2024; 9(2): 159–174. https://doi.org/10.1007/s40974-023-00296-3.
[34] Cheah CB, Samsudin MH, Ramli M, Ken PW, Tan LE. The use of high calcium wood ash in the preparation of Ground Granulated Blast Furnace Slag and Pulverized Fly Ash geopolymers: a complete microstructural and mechanical characterization. Journal of Cleaner Product 2017; 156: 114–23. https://doi.org/10.1016/j.jclepro.2017.04.026.
[35] Criado M, Fernández-Jiménez A, de la Torre AG, Aranda MAG, Palomo A. An XRD study of the effect of the $SiO_2/Na_2O$ ratioon the alkali activation of fly ash. Cement and Concrete Research 2007; 37(5): 671-679. https://doi.org/10.1016/j.cemconres.2007.01.013.
[36] Ulian G, Valdrè G. Structural and elastic behaviour of sodalite $Na_8(Al_6Si_6O_{24})Cl_2$ at high-pressure by first-principle simulations. Minerals 2022;12: 1323. https://doi.org/10.3390/min12101323.
[37] Wang Q, Li H, Ding Z, Shan R, Zhao M. Construction of a molecular dynamics model of N-A-S-H geopolymer based on XRD analysis. Materials 2024, 17, 6103. https://doi.org/10.3390/ma17246103.
[38] Chindaprasirt P, Sriopas B, Phosri P, Yoddumrong P, Anantakarn K, Kroehong W. Hybrid high calcium fly ash alkali-activated repair material for concrete exposed to sulfate environment. Journal of Building Engineering 2022, 45, 103590. https://doi.org/10.1016/j.jobe.2021.103590.
[38] Perez-Cortes P, Garcia-Lodeiro I, Puertas F, Alonso MC. Effect of incorporating a molten salt waste from nuclear power plants on the properties of geopolymers and Portland cement waste forms. Cement and Concrete Composites 2023; 142: 105210. https://doi.org/10.1016/j.cemconcomp.2023.105210.
[39] Dung NT, Hooper TJN, Unluer C. Accelerating the reaction kinetics and improving the performance of $Na_2CO_3$- activated GGBS mixes. Cement and Concrete Research (2019); 126: 105927. https://doi.org/10.1016/j.cemconres.2019.105927.
[40] Chindaprasirt P, De Silva P, Sagoe-Crentsil K, Hanjitsuwan S. Effect of $SiO_2$ and $Al_2O_3$ on the setting and hardening of high calcium fly ash-based geopolymer systems. Journal of Materials Science (2012); 47: 4876–4883. https://doi.org/10.1007/s10853-012-6353-y.
[41] Juengsuwattananon K, Winnefeld F, Chindaprasirt P, Pimraksa K. Correlation between initial $SiO_2/Al_2O_3$, $Na_2O/Al_2O_3$, $Na_2O/SiO_2$ and $H_2O/Na_2O$ ratios on phase and microstructure of reaction products of metakaolin-rice husk ash geopolymer. Construction and Building Materials (2019); 226: 406-417. https://doi.org/10.1016/j.conbuildmat.2019.07.146.